Available online at www.sciencedirect.com
SCIENCE DIRECT®
Journal of Solid State Chemistry 178 (2005) 3218–3232
JOURNAL OF SOLID STATE CHEMISTRY
www.elsevier.com/locate/jssc

Crystal structures of $Rb_2U_2O_7$ and $Rb_8U_9O_{31}$, a new layered rubidium uranate

S. Yagoubi, S. Obbade*, C. Dion, F. Abraham

Laboratoire de Cristallochimie et Physicochimie du Solide, UMR CNRS 8012, ENSCL-USTL, B.P. 90108, 59652 Villeneuve d'Ascq Cedex, France

Received 30 May 2005; received in revised form 18 July 2005; accepted 19 July 2005
Available online 16 September 2005

Abstract

Two alkali metal uranates $Rb_2U_2O_7$ and $Rb_8U_9O_{31}$ have been synthesized by solid state reaction at high temperature and their crystal structures determined from single crystal X-ray diffraction data, collected with a three circles Brucker SMART diffractometer equipped by Mo($K\alpha$) radiation and a charge-coupled device (CCD) detector. Their structures were solved using direct methods and Fourier difference techniques and refined by a least-square method on the basis of F^2 for all unique reflections, with $R_1 = 0.043$ for 53 parameters and 746 independent reflections with $I \geqslant 2\sigma(I)$ for $Rb_2U_2O_7$, monoclinic symmetry, space group $P2_1/c$, $a = 7.323(2)$ Å, $b = 8.004(3)$ Å, $c = 6.950(2)$ Å, $\beta = 108.81(1)^\circ$, $\rho_{mes} = 6.56(3)\,g/cm^3$, $\rho_{cal} = 6.54(2)\,g/cm^3$, $Z = 2$ and $R_1 = 0.036$ for 141 parameters and 2065 independent reflections with $I \geqslant 2\sigma(I)$ for $Rb_8U_9O_{31}$, orthorhombic, space group *Pbna*, $a = 6.9925(9)$ Å, $b = 14.288(2)$ Å, $c = 34.062(5)$ Å, $\rho_{mes} = 6.47(3)\,g/cm^3$, $\rho_{cal} = 6.48(2)\,g/cm^3$, $Z = 4$.

The $Rb_2U_2O_7$ structure presents a strong analogy with that of $K_2U_2O_7$ and can be described by layers of distorted $UO_2(O_4)$ octahedra built from dimeric units of edge shared octahedra further linked together by opposite corners. In $Rb_8U_9O_{31}$ puckered layers are formed by the association of two different uranium polyhedra, pentagonal bipyramids and distorted octahedra. The structure of $Rb_8U_9O_{31}$ is built from a regular succession of $^1_\infty[U_4O_{14}]^{4-}$ infinite ribbons similar to those observed in diuranates $M_2U_2O_7$ (M = K, Rb) and infinite three polyhedra wide ribbons $^1_\infty[U_5O_{21}]^{12-}$, to create an original undulated sheets $^2_\infty[U_9O_{31}]^{8-}$.

For both compounds Rb^+ ions occupy the interlayer space and exhibit comparable mobility with conductivity measurements indicating an Arrhenius-type behavior.

Keywords: Rubidium uranate; Solid state synthesis; Crystal structure refinement; Layered compound; Cationic conductivity

1. Introduction

The uranates in general and particularly those of alkali metals form a very important family of uranium compounds. If one considers only the alkali metal uranates containing uranium in its highest oxidation state U^{6+}, frequently observed, several compounds are described in the literature and can be definite by the molar ratio $n = UO_3/M_2O$ (M = alkali metal), where n presents numerous values in a large range from 0.33 to 15 (Table 1). The majority of these compounds were recently given by Griffiths and Volkovich in an extensive review [1], where the alkali metal uranates (VI) have been examined in details and their structural, physical, thermodynamic and spectroscopic properties were considered. However, an important first report of Van Egmond [2], containing at the same time a critical assessment of previous powder works and the results of many structural studies carried out mainly by powder X-ray diffraction data, give a good synthetic view of these compounds. A particular attention was devoted to cesium uranates in reason of their potential formation in nuclear reactors by reaction of UO_3, resulting of UO_2 oxidation, with cesium obtained by fission reactions [2–5].

Following these studies, it was observed that the most known uranates are the monouranates M_2UO_4, which

*Corresponding author. Fax: +33 3 20 43 68 14.
E-mail addresses: said.obbade@ensc-lille.fr, obbade@ensc-lille.fr (S. Obbade).

0022-4596/$ - see front matter © 2005 Elsevier Inc. All rights reserved.
doi:10.1016/j.jssc.2005.07.017

Table 1
The established alkali metal uranate compounds

UO_3/M_2O ratio	Formulae	Li	Na	K	Rb	Cs
15	$M_2U_{15}O_{46}$					$Cs_2U_{15}O_{46}$
7	$M_2U_7O_{22}$			$K_2U_7O_{22}$	$Rb_2U_7O_{22}$	$Cs_2U_7O_{22}$
5	$M_2U_5O_{16}$					$Cs_2U_5O_{16}$
4	$M_2U_4O_{13}$			$K_2U_4O_{13}$	$Rb_2U_4O_{13}$	$Cs_2U_4O_{13}$
3	$M_2U_3O_{10}$	$Li_2U_3O_{10}$				
2,5	$M_4U_5O_{17}$					$Cs_4U_5O_{17}$
2,25	$M_8U_9O_{31}$				**$Rb_8U_9O_{31}$**[a]	
2	$M_2U_2O_7$		$Na_2U_2O_7$	$K_2U_2O_7$	**$Rb_2U_2O_7$**[a]	$Cs_2U_2O_7$
1,33	$M_6U_4O_{15}$			$K_9U_6O_{22.5}$		
1	M_2UO_4	Li_2UO_4	Na_2UO_4	K_2UO_4	Rb_2UO_4	Cs_2UO_4
0,5	M_4UO_5	Li_4UO_5	Na_4UO_5	K_4UO_5		
0,33	M_6UO_6	Li_6UO_6 $Li_4K_2UO_6$		$Li_4K_2UO_6$		

[a]This study.

exist for all the alkali metals, and the diuranates $M_2U_2O_7$ [2–20], and that the increase of alkali metal atoms size supports the formation of uranates with higher n values. Thus, $M_2U_4O_{12}$, $M_2U_4O_{13}$ and $M_2U_7O_{22}$ are obtained only for heavy alkali metals $M = K$, Rb, Cs [3,5–8,11,21,22] and only the cesium compound $Cs_2U_{15}O_{46}$ [3,5] illustrates the highest n value found in a polyuranate after invalidation of $Cs_2U_{16}O_{49}$ [3]. Moreover, for cesium element, specific compounds are observed such as $Cs_4U_5O_{17}$ [3,5–7] and $Cs_2U_5O_{16}$ [3] which do not exist for the other alkali metals. Inversely, small alkali metals generate basic uranates with $n<1$, for example $n = 0.50$ is illustrated by M_4UO_5 with $M =$ Li, Na, K and $n = 0.33$ is represented by Li_6UO_6 and $Li_4K_2UO_6$ [23–26].

Concerning rubidium uranates, only the five compounds Rb_2UO_4, $Rb_2U_2O_7$, $Rb_2U_4O_{12}$, $Rb_2U_4O_{13}$, and $Rb_2U_7O_{22}$ have been found to exist and the indexing of powder X-ray diffraction data evidenced that these compounds are probably isostructural to the corresponding potassium uranates [9,11,12,17,22].

Alkali metal uranate compounds are generally obtained by high temperature synthesis and for each uranates family the thermal stability decreases with alkali metal size [3–5,9,10,22,27,28]. Thus, the diuranates are generally considered to present the highest thermal stability and remain stable beyond 1300 °C. On the other hand, if lithium monouranate Li_2UO_4 does not change at 1300 °C, the corresponding sodium and potassium compounds decompose in air at 1200–1300 °C to give a mixture of diuranate and alkali metal oxide. However, the generally high melting points explain the difficulties to obtain single crystals, thus, numerous structural studies have been undertaken by Rietveld method using powder X-ray diffraction data and more recently neutron diffraction.

Most of the alkali metal uranates structures are built from uranium–oxygen layers. Thus, the bi-dimensional character of these structures confers them remarkable properties in the domains of insertion, exchanges and electrical ionic conductivity, in relation with the cationic mobility of the alkali ions located in the space between layers. Thus, in the formed sheets, the linear uranyl ion $[O=U=O]^{2+}$ is surrounded in the equatorial plane by four, five or more rarely six oxygen atoms to form octahedra $(UO_2)O_4$, pentagonal bipyramids $(UO_2)O_5$ or hexagonal bipyramids $(UO_2)O_6$, respectively. The uranyl polyhedra are associated in equatorial planes by sharing corners and/or edges of oxygen atoms to form varied types of sheets. The crystal structure stability is assured by interlayer alkali metal ions. For alkali metal monouranate families $M_{2m+2}UO_{4+m}$ with $m = 0$, 1 and 2 corresponding to M_2UO_4, M_4UO_5 and M_6UO_6, respectively, different structural types depending on the uranium polyhedra polymerisation degree have been reported [1,5,8,11–14,25,26]. Thus, for the monouranate family M_2UO_4, the crystal structure is obtained by association of $U(O_2)O_4$ octahedra sharing all equatorial corners to build infinite sheets $^2_\infty[(UO_2)O_2]^{2-}$, except in α-Na_2UO_4 where the octahedra are associated by two opposite equatorial edges to form infinite chains $^1_\infty[(UO_2)O_2]^{2-}$, however, in M_4UO_5 compounds, a decondensation of uranyl polyhedra is observed and the $U(O_2)O_4$ octahedra share only two opposites corners to form infinite chains $^1_\infty[(UO_2)O_3]^{4-}$. Finally independent octahedra $(UO_6)^{6-}$ are found in ultimate term of decondensation in the structure of Li_6UO_6. When the molar ratio n is higher than 1, as in polyuranates, an increase of uranyl polyhedra condensation is observed to give denser sheets. For example, in diuranates $M_2U_2O_7$ ($n = 2$), the $U(O_2)O_4$ octahedra are sharing an equatorial edge to create dimeric units U_2O_{10} linked together by different ways to form various layers. For higher n values, the condensation is still more accentuated and uranium atoms adopt two different environments, $(UO_2)O_5$ pentagonal bipyramids and $(UO_2)O_4$

distorted octahedra, which are associated in complex layered structures.

Owing to the difficulty to obtain single crystals of alkali metal uranates, for most compounds only X-ray powder diffraction studies were carried out until now. Thus, for $Rb_2U_2O_7$, only one crystal structure determination using powder X-ray diffraction data and Rietveld method refinement has been reported by Van Egmond [2]. In the same way, different unit cell parameters have been reported for monoclinic [3,9], rhombohedral [12] and orthorhombic symmetries [29].

This work is dedicated to the crystal structure, thermal, electrical and spectroscopic investigations of two rubidium uranates, the new phase $Rb_8U_9O_{31}$ and the diuranate $Rb_2U_2O_7$. Both compounds were synthesized by solid-state reaction at high temperature and their structures were determined using single crystal X-ray diffraction data. The results concerning the $Rb_2U_2O_7$ structure are compared with the potassium and cesium diuranates, previously established from powder X-ray diffraction data. Conductivity and infrared measurements are reported for both compounds.

2. Experimental

2.1. Powder samples preparation and characterization

Polycrystalline samples of $Rb_2U_2O_7$ and $Rb_8U_9O_{31}$ were prepared by conventional solid-state reactions at high temperature, using pure initial materials $RbNO_3$ (Adrich) and U_3O_8 (Prolabo) as reagents. Mixture of starting materials in the appropriate stoichiometries were heated at 750 °C in air for 2 days with intermediate grindings for $Rb_2U_2O_7$. For $Rb_8U_9O_{31}$, a thermal treatment at 900 °C during 3 weeks has been necessary to obtain a pure sample.

The end of the synthesis process for each sample was controlled by powder X-ray diffraction using a Guinier–De Wolff focusing camera and Cu$K\alpha$ radiation.

Powder X-ray diffraction data used for cell parameters refinement were recorded on a Siemens D5000 $\theta/2\theta$ diffractometer, at room temperature, using Bragg–Brentano geometry, with a back-monochromatized Cu$K\alpha$ radiation. The diffraction pattern was scanned over the angular range 05–80°(2θ) in step of 0.03°(2θ) and a counting time of 15 s per step. The unit cell parameters were refined by a least-squares procedure from the indexed powder diffraction pattern, using Rietveld method.

Synthesis attempts of $Rb_8U_9O_{31}$ isotypic compounds with other alkali metals by solid state reactions have been investigated from mixtures of MNO_3 (M = K, Cs) and U_3O_8 in molar ratio 8/3, corresponding to $M_8U_9O_{31}$. The mixtures were slowly heated (1°/min), in platinum crucibles, and maintained 3 days at different temperatures between 600 and 1200 °C with intermediate grindings. For both alkali metals no $M_8U_9O_{31}$ was observed in the 600–1200 °C temperature range. For the potassium preparation, the X-ray powder analysis of the sample at different temperatures evidenced the formation of two known phases $K_2U_2O_7$ and $K_2U_4O_{13}$, which are stable until 1200 °C. For the cesium sample, the formation of $Cs_4U_5O_{17}$ accompanied with cesium oxide Cs_2O was confirmed by powder X-ray diffraction.

The densities were measured with an automated Micromeritics Accupy 1330 helium pycnometer using a 1-cm^3 cell.

For both compounds, differential thermal analysis (DTA) was carried out in air on a Setaram 92-1600 thermal analyzer in the temperature range 20–1300 °C with heating and cooling rate 1.5 °C/min using platinum crucibles.

For conductivity measurements, powder samples were palletized at room temperature using a conventional cold press and then sintered at 800 °C for 15 h. For each sample, gold electrodes were sputtered on both flat faces and measurements were done by impedance spectrometry in the frequency range 1–10^6 Hz using a Schlumberger 1170 frequency response analyzer. Each set of values was recorded in temperature range 200–600 °C with a step of 20 °C and for every measurement the temperature was stabilized during 1 h.

To characterize the vibration modes of uranium atoms in both compounds, the infrared spectra were recorded using the KBr dispersion technique (1 mg of sample in 120 mg KBr) and a Bruker Vector 22 Fourier transform infrared spectrometer, which covers the range 400–4000 cm^{-1}.

2.2. Crystal growth

The single crystals of $Rb_2U_2O_7$ and $Rb_8U_9O_{31}$ were obtained during studies relating to the ternary system Rb_2O–U_3O_8–MoO_3, starting from a molar ratio Mo/U = 2/1, in an excess of rubidium carbonate Rb_2CO_3 (10 mole for 2 mole of MoO_3). In a first experiment, the mixture was heated in a platinum crucible at 940 °C for 3 h and then slowly cooled to room temperature at 0.2 °C/min. The product of the reaction was washed with water to remove Rb_2CO_3 excess and filtered, giving a two-phases sample containing a small quantity of orange single crystals of $Rb_8U_9O_{31}$ and a majority of twinned yellow crystals corresponding to $Rb_2U_2MoO_{10}$ which is isotypic to the recently characterized $K_2U_2MoO_{10}$ [30]. The second crystallization experiment carried out on a mixture with the same molar ratio 2/1 heated at 1200 °C, then slowly cooled (0.3 °C/min), allowed the growth of orange crystals of rubidium diuranate $Rb_2U_2O_7$, once again accompanied by yellow crystals of $Rb_2U_2MoO_{10}$.

2.3. Crystal structures determination

Appropriate single crystals of $Rb_2U_2O_7$ and $Rb_8U_9O_{31}$ with dimensions $0.180 \times 0.080 \times 0.054$ mm and $0.070 \times 0.020 \times 0.030$ mm, respectively, were selected for X-ray diffraction analyses. Data collections were performed at 293(2) K on a Bruker X-ray diffractometer with graphite monochromated Mo$K\alpha$ radiation ($\lambda = 0.71073$ Å) and equipped with a SMART charge-coupled device (CCD) detector, with a crystal to detector distance of 5.0 cm. For both compounds, SMART was also used to determine the preliminary cell parameters from 120 frames obtained with an exposure time of 20 s per frame. For each crystal structure determination, a total of 1800 individual frames were collected using a ω-scan technique with an ω rotation of 0.3° and an acquisition time of 40 s per frame. Integral intensities were extracted from the collected frames with the Bruker Saint Plus 6.02 software package [31] using a narrow-frame integration algorithm. For each compound, a Gaussian-type absorption correction based on precise faces indexing was then applied using XPREP program of the SHELXTL package [32] followed by SADABS [33] for additional corrections. The crystal structures were solved by a combination of direct methods and difference Fourier syntheses, and refined by full matrix least squares against F^2, using SHELXS program [34]. The heavy atoms, U and Rb, were localized from the direct methods. The positions of oxygen atoms were deduced from subsequent refinements and difference Fourier syntheses using the SHELXL option of the SHELXTL software [32]. For both compounds, the summaries of the crystal data and details concerning the intensity data collections and structure refinements are given in Table 2.

For both compounds, the bond valence sums of the atoms have been calculated using parameters given by Brese and O'Keeffe's for Rb^+–O ($R_{ij} = 2.260$ Å and $b = 0.37$ Å) [35] and coordination-independent parameters given by Burns et al. for U^{6+}–O ($R_{ij} = 2.051$ Å and $b = 0.519$ Å) [36].

Table 2
Crystal data, intensity collection and structure refinement parameters for $Rb_2U_2O_7$ and $Rb_8U_9O_{31}$

	$Rb_2U_2O_7$	$Rb_8U_9O_{31}$
Crystal data		
Crystal symmetry	Monoclinic	Orthorhombic
Space group	$P2_1/c$	*Pbna*
Unit cell (from single crystal)	$a = 7.323(2)$ Å	$a = 6.9925(9)$ Å
	$b = 8.004(3)$ Å	$b = 14.2884(19)$ Å
	$c = 6.950(2)$ Å	$c = 34.062(5)$ Å
	$\beta = 108.8(1)°$	
	$V = 385.6(2)$ Å^3	3403.2(8) Å^3
Z	2	4
Calculated density	$\rho_{cal} = 6.54(2)$ g cm^{-3}	$\rho_{cal} = 6.48(2)$ g cm^{-3}
Measured density	$\rho_{mes} = 6.56(3)$ g cm^{-3}	$\rho_{mes} = 6.47(3)$ g cm^{-3}
Color	Orange	Orange
Data collection		
Temperature (K)	293(2)	293(2)
Radiation Mo($K\alpha$)	0.71073 Å	0.71073 Å
Scan mode	ω	ω
Recording angular range (°)	4.01/29.15	2.85/30.01
Recording reciprocal space	$-9 \leqslant h \leqslant 9$	$-9 \leqslant h \leqslant 9$
	$-10 \leqslant k \leqslant 10$	$-19 \leqslant k \leqslant 19$
	$-9 \leqslant h \leqslant 9$	$-46 \leqslant l \leqslant 47$
Number of reflections		
Measured/independent	2211/746	12134/2065
Absorption, μ (cm^{-1})	544.70	541.26
Refinement		
Refined Parameters/ restraints	53/0	141/0
Goodness of fit on F^2	1.117	1.041
$R_1[I > 2\sigma(I)]$	0.0432	0.0365
$wR_2[I > 2\sigma(I)]$	0.0982	0.0702
Largest diff. Peak and hole (e Å^{-3})	3.011/−3.810	2.155/−2.925

Note: $R_1 = \sum(|F_o| - |F_c|)/\sum|F_o|$
$wR_2 = [\sum w(F_o^2 - F_c^2)^2 / \sum w(F_o^2)^2]^{1/2}$.
$w = 1/[\sigma^2(F_0^2) + (aP)^2 + bP]$ where a and b are refinable parameters and $P = (F_o^2 + 2F_c^2)/3$.

3. Results and discussion

3.1. Structure solution

Systematic absences of reflections were consistent with $P2_1/c$ and *Pbna* centrosymmetric space groups for $Rb_2U_2O_7$ and $Rb_8U_9O_{31}$, respectively. The indexed powder patterns and refined cell parameters are reported in the Tables 3 and 4 for $Rb_2U_2O_7$ and $Rb_8U_9O_{31}$, respectively. The reliability of the unit cell refinement and indexing reflections is indicated by the conventional figures of merit F_{20}, defined by Smith and Snyder [37], $F_{20} = 36$ (0.0155; 36) and 44 (0.0115; 46) for $Rb_2U_2O_7$ and $Rb_8U_9O_{31}$, respectively. A good agreement is observed between calculated and measured densities for both compounds, with two formulas per unit cell ($\rho_{mes} = 6.56(3)$ g cm^{-3}, $\rho_{cal} = 6.54(2)$ g cm^{-3}) for $Rb_2U_2O_7$ and four formulas per unit cell ($\rho_{mes} = 6.47(3)$ g cm^{-3}, $\rho_{cal} = 6.48(2)$ g cm^{-3}) for $Rb_8U_9O_{31}$. Refinement of atomic positional parameters and anisotropic displacement parameters for all atoms yielded to final $R_1 = 0.0432$ and $wR_2 = 0.0982$ for 746 independent reflections for $Rb_2U_2O_7$ and $R_1 = 0.0365$, $wR_2 = 0.0702$ for 2065 independent reflections for $Rb_8U_9O_{31}$. The atomic positions with equivalent isotropic displacement parameters are reported in Tables 5 and 6, anisotropic displacement parameters are given in Tables 7 and 8 for $Rb_2U_2O_7$ and $Rb_8U_9O_{31}$, respectively.

3.2. Description of the structure of $Rb_2U_2O_7$

The selected interatomic distances and O–U–O angles are reported in Table 9 for $Rb_2U_2O_7$.

Table 3
Observed and calculated powder X-ray diffraction pattern for $Rb_2U_2O_7$

h	k	l	$2\theta_{obs}$	$2\theta_{cal}$	I (%)	h	k	l	$2\theta_{obs}$	$2\theta_{cal}$	I (%)
1	0	0	12.76	12.76	35	3	1	1	47.04	47.02	2
0	1	1	17.44	17.45	1	−2	2	3	47.08	47.12	7
−1	1	1	18.89	18.92	1	1	4	0	47.22	47.25	7
1	1	1	24.14	24.13	2	0	2	3	47.24	47.26	9
2	0	0	25.68	25.67	50	1	1	3	48.73	48.74	4
0	2	1	26.04	26.05	26	−4	0	2	51.00	51.06	15
−1	2	1	27.06	27.08	100	−4	1	1	51.25	51.27	28
0	0	2	27.09	27.11	45	−3	2	3	52.56	52.61	22
−1	1	2	28.28	28.28	5	4	0	0	52.78	52.78	23
0	1	2	29.33	29.36	3	1	2	3	52.84	52.85	18
−2	0	2	30.83	30.86	29	−1	0	4	52.86	52.92	2
1	2	1	31.01	31.02	58	−1	4	2	52.93	52.96	7
−2	1	2	32.85	32.90	1	−2	0	4	53.36	53.42	9
−2	2	1	33.57	33.59	7	0	4	2	53.56	53.58	25
1	0	2	33.69	33.69	1	−2	4	2	55.79	55.83	19
3	0	0	38.95	38.94	8	0	0	4	55.86	55.90	6
2	2	1	39.99	39.98	6	0	1	4	57.13	57.18	3
−1	1	3	40.52	40.52	8	1	4	2	57.61	57.62	3
1	3	1	40.14	40.15	1	2	1	3	57.64	57.63	1
−1	1	3	40.52	40.57	6	3	3	1	57.77	57.76	1
−2	1	3	42.56	42.62	1	1	3	3	59.24	59.25	2
0	1	3	42.72	42.76	2	−4	2	3	60.96	61.02	6
−3	2	1	43.40	43.43	38	3	4	0	61.22	61.23	5
−3	2	1	43.58	43.56	16	−3	4	2	61.82	61.87	3
0	3	2	43.65	43.67	2	4	2	1	64.14	64.11	4
2	1	2	45.10	45.08	2	−4	0	4	64.24	64.30	4
−1	2	3	45.20	45.25	41	2	4	2	64.66	64.65	13
3	2	0	45.28	45.28	24	−2	5	2	66.76	66.74	3

$a = 7.3182(3)$, $b = 8.0027(3)$, $c = 6.9385(2)$, $\beta = 108.68(1)^\circ$ $F_{20} = 36(0.0155; 36)$.

The crystal structure of $Rb_2U_2O_7$ contains only one U^{6+} uranium cation strongly bonded to two oxygen atoms O(1) and O(2) at shorter distances 1.848(10) and 1.851(11) Å, respectively, giving nearly linear uranyl ion $(UO_2)^{2+}$ [O(1)–U–O(2) = 178.7(5)°]. The uranyl ion is coordinated by four additional oxygen atoms (three O(3) and one O(4)) located at the equatorial vertices of a distorted octahedron. The U–O average bond lengths value 2.25(1) Å corresponding to the equatorial oxygen atoms, ranging from 2.150(10) to 2.284(12) Å, is in good agreement with the average bond lengths of 2.28(5) Å determined by Burns et al. [36] from numerous well refined structures containing uranyl ions in tetragonal bipyramid coordination.

The structure can be described starting from centrosymmetric dimeric units $[U_2O_{10}]^{8-}$ created by two octahedra sharing O(3)–O(3) edges. These dimeric units are connected together by opposite O(4) corners to develop parallel infinite chains $^1_\infty[U_2O_9]^{6-}$ running along the $\vec{c}$-axis. The neighbouring $^1_\infty[U_2O_9]^{6-}$ infinite chains are associated by sharing all O(3) corners to create infinite $^2_\infty[U_2O_7]^{2-}$ sheets parallel to (100) plane, Fig. 1a, comparable to those observed in $K_2U_2O_7$ described in the non-centrosymmetric space group $P2_1$ [20], however in this compound the uranium coordination one uranium atom is completed by a long U–O distance ($d_{U-O} = 2.89$ Å) to give a pentagonal bipyramid. In the present arrangement, each O(4) oxygen atom is common to two $UO_2(O_4)$ deformed octahedra whereas each O(3) oxygen atom is shared between three uranium octahedra, to give empty triangles O(3)–O(3)–O(4). Similar $[U_2O_{10}]^{8-}$ dimers are also observed in $Cs_2U_2O_7$. In this compound the dimers are connected by sharing two *trans* edges to create infinite chains $^1_\infty[U_2O_8]^{4-}$ running along *b*-axis. These chains are themselves linked together by sharing corners to form $^2_\infty[U_2O_7]^{4-}$ layers parallel to (100), Fig. 1c, with Autunite-type sheet anion topology but with an original occupation of the squares not found in mineral structures [38] (Fig. 1d).

The Rb^+ rubidium ions occupy the interlayer space and ensure the cohesion of the structure (Fig. 2a). Thus, the unique independent rubidium atom Rb is surrounded by six oxygen atoms in the range 2.774(11)–2.911(12) that form a distorted octahedral environment (Fig. 2b). All the Rb–O distances lower than 3.0 Å involve only oxygen atoms of uranyl ions. Each rubidium octahedron is edge shared to six neighboring octahedra to form a very dense RbO_2 layers in (100) plane similar to those found, for example, in the CdI_2-type structure (Fig. 2c). Thus the structure

Table 4
Observed and calculated X-ray powder diffraction pattern for $Rb_8U_9O_{31}$

h	k	l	$2\theta_{obs}$	$2\theta_{cal}$	I (%)	h	k	l	$2\theta_{obs}$	$2\theta_{cal}$	I (%)	h	k	l	$2\theta_{obs}$	$2\theta_{cal}$	I (%)
0	2	0	12.38	12.36	17	2	4	0	35.91	35.93	2	1	7	5	48.29	48.32	8
0	2	1	12.65	12.66	66	2	4	2	36.31	36.33	2	1	6	10	48.38	48.41	8
0	2	2	13.43	13.44	15	1	4	9	36.88	36.90	4	3	3	8	48.41	48.43	8
1	1	5	19.20	19.21	3	1	1	13	37.15	37.17	2	1	5	13	48.89	48.91	4
1	1	6	21.08	21.09	3	0	6	1	37.84	37.86	4	2	3	14	49.45	49.47	2
0	2	7	22.09	21.10	2	0	6	3	38.60	38.62	7	2	2	15	49.49	49.52	8
1	3	2	23.17	23.18	2	1	4	10	38.70	38.72	2	3	3	9	49.72	49.75	2
1	3	3	23.91	23.92	2	0	2	14	39.09	39.10	2	0	2	18	49.81	49.84	15
1	3	4	24.90	24.91	1	0	6	4	39.25	39.27	7	0	4	16	49.82	49.85	10
0	4	0	24.91	24.92	7	0	6	5	40.09	40.10	4	3	4	7	50.32	50.35	13
0	4	1	25.04	25.06	9	1	4	11	40.63	40.65	19	2	1	16	50.56	50.59	5
1	1	8	25.25	25.26	5	2	5	1	40.89	40.90	13	0	8	0	51.10	51.13	6
2	0	0	25.46	25.46	7	2	5	2	41.11	41.13	2	3	3	10	51.17	51.20	16
0	4	2	25.46	25.47	61	1	6	4	41.40	41.42	3	0	8	0	51.40	51.43	5
1	2	7	25.53	25.54	22	3	2	3	41.49	41.50	2	1	2	18	51.61	51.63	5
2	0	2	25.99	26.00	3	2	5	3	41.55	41.57	10	2	2	12	51.65	51.68	5
1	3	5	26.12	26.14	2	1	5	9	41.62	41.64	3	3	5	4	51.69	51.72	6
0	4	3	26.13	26.15	30	0	2	15	41.70	41.72	6	1	6	12	51.74	51.77	11
2	1	0	26.22	26.23	43	2	4	8	41.89	41.91	3	0	6	13	51.84	51.87	5
2	1	1	26.35	26.36	20	2	5	4	42.16	42.18	8	0	8	4	52.29	52.32	7
0	2	9	26.63	26.65	3	1	6	5	42.19	42.22	12	3	2	12	52.34	52.36	5
2	1	2	26.75	26.76	10	1	4	12	42.65	42.68	7	3	5	5	52.36	52.39	12
1	0	9	26.76	26.78	100	2	2	12	42.91	42.93	2	2	7	3	52.49	52.52	3
0	4	4	27.05	27.06	6	2	5	5	42.94	42.96	3	3	0	13	52.50	52.53	4
2	1	3	27.39	27.40	1	3	0	7	42.99	43.01	7	4	0	2	52.59	52.60	3
1	1	9	27.49	27.51	46	1	6	6	43.14	43.17	16	0	2	19	52.59	52.62	10
1	2	8	27.50	27.51	74	1	5	10	43.27	43.29	3	4	1	0	52.71	52.73	14
1	3	6	27.55	27.57	25	3	1	7	43.48	43.50	10	3	3	11	52.74	52.76	12
2	0	4	27.56	27.57	3	3	2	6	43.82	43.84	5	0	8	5	52.96	52.92	12
2	1	4	28.27	27.28	3	0	2	16	44.36	44.39	13	2	7	4	53.01	53.04	6
2	2	0	28.40	28.41	13	3	1	8	44.74	44.76	28	2	1	17	53.02	53.05	5
2	2	1	28.52	28.53	58	1	4	13	44.78	44.80	2	3	5	6	53.17	53.20	13
2	2	2	28.89	28.90	15	1	5	11	45.04	45.06	3	4	0	4	53.47	53.49	6
1	3	7	29.16	29.17	23	1	6	8	45.49	45.52	9	1	8	3	53.52	53.55	5
1	2	9	29.58	29.60	26	3	0	9	45.68	45.69	5	1	6	13	53.59	53.62	5
1	1	10	29.81	29.83	8	2	1	14	45.84	45.86	3	2	7	5	53.66	53.69	7
1	3	8	30.91	30.93	9	3	1	9	46.14	46.16	46	0	8	6	53.76	53.76	10
1	4	5	31.00	31.02	2	2	6	1	46.16	46.18	10	0	6	14	53.82	53.86	9
2	3	0	31.72	31.74	2	3	3	6	46.18	46.20	2	2	3	16	53.93	53.96	3
1	2	10	31.77	31.78	39	1	2	16	46.32	46.34	3	4	2	0	53.96	53.98	4
2	3	1	31.83	31.85	19	2	6	3	46.81	46.83	14	1	8	4	54.03	54.06	10
2	3	2	32.17	32.18	7	1	5	12	46.91	46.83	14	3	4	10	54.05	54.08	4
1	1	11	32.20	32.22	2	1	7	3	47.02	47.05	5	3	5	7	54.12	54.14	5
1	4	6	32.23	32.25	13	0	2	17	47.07	47.09	12	2	2	17	54.26	54.29	10
2	3	3	32.71	32.73	7	1	0	17	47.15	47.17	3	3	3	12	54.41	54.44	5
2	0	8	33.13	33.14	2	3	3	7	47.22	47.24	4	2	7	6	54.46	54.49	4
1	4	7	33.63	33.65	23	2	6	4	47.37	47.39	8	2	4	15	54.56	54.59	4
2	2	7	33.95	33.96	2	1	0	17	47.40	47.43	3	4	2	3	54.60	54.63	12
1	2	11	34.02	34.05	7	1	7	4	47.58	47.61	8	1	8	5	54.68	54.71	5
1	1	12	34.65	34.67	2	0	0	18	48.02	48.07	17	0	4	18	54.86	54.89	3
1	4	8	35.19	35.21	2	2	6	5	48.08	48.11	3	2	0	18	55.14	55.17	14

$a = 6.990(2)$ Å, $b = 14.280(3)$, $c = 34.044(5)$ Å, $F_{20} = 44(0.01154; 43)$.

can be considered as the stacking along [100] of two alternating dense layers of UO_6 and RbO_6 octahedra (Fig. 3a). In fact the structure of $M_2U_2O_7$, $M = K$, Rb compounds can be described as a stacking of hexagonal type layers of oxygen atoms parallel to the (100) plane in the sequence AABBCC found, for example, in the 3*R* polytype of the molybdenite MoS_2 compound [39] in which the *M* atoms occupy the octahedral sites created by two different successive oxygen layers to form a AA*c*BB*a*CC*b* sequence where the minus letter denote *M* layers. The interspace between two successive identical oxygen layers, AA for example, is occupied by a $UO_{1.5}$

Table 5
Atomic coordinates and equivalent displacement parameters (Å^2) for $Rb_2U_2O_7$

Atom	Site	x	y	z	U_{eq}
U	4*e*	0.99385(7)	0.62403(12)	0.22357(7)	0.0130(2)
Rb	4*e*	0.4929(2)	0.8827(3)	0.2280(2)	0.0216(4)
O1	4*e*	0.2602(14)	0.6343(14)	0.3096(15)	0.019(2)
O2	4*e*	0.7268(15)	0.6190(14)	0.1377(16)	0.023(2)
O3	4*e*	0.0145(16)	0.3615(12)	0.1074(16)	0.022(2)
O4	2*a*	0	1/2	1/2	0.033(8)

Note: The U_{eq} values are defined by $U_{eq} = 1/3(\sum_i \sum_j U_{ij} a_i^* a_j^* a_i a_j)$.

Table 6
Atomic coordinates and equivalent displacement parameters (Å^2) for $Rb_8U_9O_{31}$

Atom	Site	x	y	z	U_{eq}
U1	4*c*	0.04867(13)	0.25000	0.00000	0.0085(2)
U2	8*d*	0.58563(10)	0.21247(5)	0.05647(2)	0.0080(2)
U3	8*d*	0.56331(10)	0.13223(6)	0.16955(2)	0.0131(2)
U4	8*d*	0.11966(9)	0.17285(5)	0.11001(2)	0.0091(2)
U5	8*d*	0.01624(10)	0.11660(6)	0.21559(2)	0.0106(2)
Rb1	8*d*	0.7400(3)	0.48597(16)	0.02708(7)	0.0225(5)
Rb2	8*d*	0.2526(3)	0.44846(16)	0.08736(7)	0.0236(5)
Rb3	8*d*	0.7832(3)	0.39441(15)	0.14707(7)	0.0230(5)
Rb4	8*d*	0.3034(3)	0.37347(17)	0.21998(7)	0.0264(5)
O1	8*d*	0.1130(17)	0.0496(9)	0.0969(4)	0.0144(3)
O2	8*d*	0.0509(17)	0.3723(10)	0.0145(4)	0.0164(32)
O3	8*d*	0.5883(17)	0.0881(10)	0.0416(5)	0.0228(40)
O4	4*c*	0.711(2)	0.25000	0.00000	0.0107(44)
O5	8*d*	0.1273(18)	0.2911(9)	0.1265(4)	0.0203(37)
O6	8*d*	0.4545(17)	0.1644(9)	0.1111(4)	0.0179(32)
O7	8*d*	0.5623(19)	0.0075(10)	0.1595(5)	0.0253(40)
O8	8*d*	0.8737(18)	0.1371(9)	0.1554(4)	0.0166(32)
O9	8*d*	0.587(2)	0.3351(10)	0.0734(5)	0.0269(39)
O10	8*d*	0.9000(18)	0.2054(10)	0.0663(4)	0.0189(35)
O11	8*d*	0.2700(18)	0.2167(9)	0.0453(4)	0.0126(33)
O12	8*d*	0.566(2)	0.2559(10)	0.1812(5)	0.0297(41)
O13	8*d*	0.6995(17)	0.1005(9)	0.2292(4)	0.0178(37)
O14	8*d*	0.0252(18)	0.9883(9)	0.2113(5)	0.0186(36)
O15	8*d*	0.2474(18)	0.1307(11)	0.1744(4)	0.0279(40)
O16	8*d*	0.0025(18)	0.2414(10)	0.2248(4)	0.0171(35)

Note. The U_{eq} values are defined by $U_{eq} = 1/3(\sum_i \sum_j U_{ij} a_i^* a_j^* a_i a_j)$.

Table 7
Anisotropic displacement parameters (Å^2) for $Rb_2U_2O_7$

Atom	U_{11}	U_{22}	U_{33}	U_{12}	U_{13}	U_{23}
U	0.0131(3)	0.0143(3)	0.0109(3)	0.0008(2)	0.0029(2)	−0.0023(3)
Rb	0.0241(9)	0.0205(9)	0.0203(7)	−0.0024(6)	0.0071(6)	0.0029(6)
O1	0.008(5)	0.027(6)	0.019(5)	0.000(5)	0.003(4)	0.002(4)
O2	0.010(5)	0.034(7)	0.026(6)	−0.008(6)	0.007(4)	−0.008(5)
O3	0.030(7)	0.012(6)	0.025(5)	−0.001(5)	0.010(4)	0.009(4)
O4	0.040(14)	0.14(2)	0.038(12)	−0.002(15)	0.011(10)	0.057(14)

Note: The anisotropic displacement factor exponent takes the form $-2\pi^2[h^2 a^{*2} U_{11} + k^2 b^{*2} U_{22} + l^2 c^{*2} U_{33} + \cdots + 2kla^* c^* U_{23}]$.

layer built from U atoms in *a* positions to form linear uranyl ions and by O(3) atoms ordered on half the trigonal sites, the O(4) atom is localized between two unoccupied trigonal sites and logically its atomic displacement is elongated towards the empty sites (Fig. 3b). This description explains the first structural approaches concerning $M_2U_2O_7$ (M = K, Rb) compounds reported in *R*3*m* trigonal symmetry [11,12,19] where the hexagonal *c* parameter represents the width of the layers sequence ($3a\sin\beta$). The $UO_{1.5}$ layer constitute an anion sheet topology not described for mineral materials in the completeness review by Burns et al. [38] and built from squares and triangles that results from the stacking of two arrowhead chains **S**, **S′**, **T** and **T′** (Fig. 1b). The uranium atoms occupy all the square sites when the triangular sites are empty.

On the basis of the U–O and Rb–O bond length values obtained from crystal X-ray structure determination, the bond valence sums were calculated to be 5.75 and 1.31 *vu* for U and Rb, respectively. Usual values, 2.17, 2.08 and 1.98 *vu* are obtained for O(1), O(2) and O(3), respectively, on the contrary for O(4) that belongs only to two U atoms with a large atomic displacement parameter the value is significantly lower, 1.71 *vu*.

3.3. Description of the structure of $Rb_8U_9O_{31}$

The selected interatomic distances and O–U–O angles are reported in Table 10 for $Rb_8U_9O_{31}$.

The structure of $Rb_8U_9O_{31}$ contains five symmetrically distinct U atoms. The composition deduced from the structure refinement indicates that all U occurs as U^{6+}, and as is typical in oxides, each U is bonded to two oxygen atoms at short distances forming a nearly linear uranyl ion UO_2^{2+}, with U–O bond lengths in the range 1.781(13)–1.848(15) Å and O–U–O bond angles in the range 174.5(6)–179.0(6). The coordination of U(2), U(3) and U(5) is completed in the equatorial plane by four oxygen atoms at intermediate distances (2.150(13)–2.298(13)) forming a distorted octahedron whereas the two other uranyl ions $U(1)O_2^{2+}$ and $U(4)O_2^{2+}$ are coordinated in equatorial planes by five oxygen atoms at distances varying in a largest range (2.189(13)–2.566(14)) to form pentagonal bipyramids. In this compound, the equatorial mean bond lengths, 2.39(2) and 2.37(1) Å for $U(1)O_2^{2+}$ and $U(4)O_2^{2+}$ in pentagonal bipyramid coordinations, and 2.21(1), 2.23(1) and 2.25(1) Å for $U(2)O_2^{2+}$, $U(3)O_2^{2+}$ and $U(5)O_2^{2+}$, respectively, in distorted tetragonal bipyramid environments are in excellent agreement with the average bond lengths of 2.37(9) and 2.28(5) Å determined from numerous well refined structures [36], for uranyl ions in pentagonal and tetragonal bipyramid coordination, respectively. The $U6^+$ valence of uranium

Table 8
Anisotropic displacement parameters (Å^2) of (U, Rb) for $Rb_8U_9O_{31}$

Atom	U_{11}	U_{22}	U_{33}	U_{12}	U_{13}	U_{23}
U1	0.0070(5)	0.0102(6)	0.0084(6)	0.00000	0.00000	0.0005(5)
U2	0.0081(3)	0.0101(4)	0.0057(4)	−0.0004(3)	0.0007(3)	0.0015(3)
U3	0.0115(4)	0.0168(4)	0.0109(4)	0.0009(3)	−0.0016(3)	0.0030(4)
U4	0.0083(3)	0.0110(4)	0.0080(4)	0.0004(3)	−0.0005(3)	0.0012(3)
U5	0.0119(4)	0.0137(4)	0.0062(3)	−0.0019(3)	−0.0001(3)	−0.0001(4)
Rb1	0.0220(11)	0.0254(13)	0.0201(14)	0.0013(9)	−0.0016(10)	−0.0022(10)
Rb2	0.0202(11)	0.0243(13)	0.0261(14)	0.0002(9)	0.0032(10)	0.0076(11)
Rb3	0.0221(11)	0.0234(13)	0.0234(14)	−0.0017(9)	0.0042(10)	−0.0012(10)
Rb4	0.0183(11)	0.0224(13)	0.0384(16)	0.0027(10)	0.004(1)	0.0050(12)
O1	0.012(7)	0.020(8)	0.011(9)	0.001(6)	0.002(6)	−0.001(7)
O2	0.016(7)	0.015(8)	0.019(8)	−0.003(7)	0.004(6)	−0.005(7)
O3	0.008(6)	0.031(10)	0.037(11)	0.008(6)	0.009(7)	−0.010(8)
O4	0.005(9)	0.027(12)	0.009(11)	0.00000	0.00000	0.007(9)
O5	0.019(8)	0.010(8)	0.031(11)	0.001(6)	0.007(7)	−0.002(7)
O6	0.023(7)	0.015(7)	0.016(9)	−0.001(6)	0.004(7)	0.002(6)
O7	0.028(9)	0.020(9)	0.028(11)	−0.003(7)	−0.007(8)	0.006(7)
O8	0.021(7)	0.020(8)	0.009(8)	0.006(7)	0.007(6)	0.010(7)
O9	0.032(9)	0.029(9)	0.02(1)	0.004(8)	0.007(7)	−0.009(7)
O10	0.010(7)	0.030(9)	0.016(9)	0.008(6)	−0.005(6)	0.000(7)
O11	0.013(7)	0.020(8)	0.012(8)	0.003(6)	−0.005(6)	0.012(6)
O12	0.045(10)	0.012(9)	0.032(11)	−0.005(8)	0.002(8)	0.003(7)
O13	0.009(7)	0.015(9)	0.034(11)	0.010(6)	−0.002(6)	−0.006(7)
O14	0.013(7)	0.016(8)	0.027(11)	0.004(6)	0.000(7)	0.001(7)
O15	0.014(7)	0.038(10)	0.031(10)	−0.001(7)	0.008(7)	0.017(9)
O16	0.021(7)	0.020(9)	0.010(9)	0.003(7)	−0.004(6)	0.001(6)

Note: The anisotropic displacement factor exponent takes the form $-2\pi^2[h^2a^{*2}U_{11} + k^2b^{*2}U_{22} + l^2c^{*2}U_{33} + \cdots + 2kla^*c^*U_{23}]$.

Table 9
Interatomic distances (Å), valence bond and uranium–oxygen angles (°) in $Rb_2U_2O_7$

	d_{U-O}	s_{ij}	Uranium–oxygen angles	
Environment of U				
U–O1	1.848(10)	1.479		
U–O2	1.852(11)	1.467	O1–U–O2	178.69(49)
U–O4	2.150(10)	0.826	O1–U–O4	90.89(32)
U–O3^{i}	2.246(10)	0.687	O1–U–O3	88.39(46)
U–O3	2.274(10)	0.651	O1–U–O3^{i}	89.83(46)
U–O3^{ii}	2.284(12)	0.638	O1–U–O3^{ii}	90.36(43)
	$\sum s_{ij}$	**5.75**		
Environment of Rb				
Rb–O1^{iv}	2.774(11)	0.251		
Rb–O1	2.793(12)	0.239		
Rb–O2^{v}	2.810(13)	0.228		
Rb–O2^{i}	2.829(12)	0.217		
Rb–O1^{iii}	2.861(12)	0.199		
Rb–O2^{vi}	2.911(12)	0.173		
	$\sum s_{ij}$	**1.31**		

Symmetry codes: (i) $-x, 0.5+y, 0.5-z$; (ii) $-x, 1-y, -z$; (iii) $x, 1.5-y, -0.5+z$; (iv) $1-x, 0.5+y, 0.5-z$; (v) $1+x, 1.5-y, 0.5+z$; (vi) $1+x, y, z$.

atoms is confirmed by the sum of the valences bonds (Table 10).

As previously observed in $M_2U_2O_7$ diuranate structures with $M = K$, Rb, the $U(3)O_6$ and $U(5)O_6$ octahedra share the O(8)–O(13) equatorial edge to create dimeric units $[U_2O_{10}]^{8-}$. These dimers are associated by sharing opposite corners O(15) to form an infinite chain $^1_\infty[U_2O_9]^{6-}$ running along the $\vec{a}$-axis. Two parallel $^1_\infty[U_2O_9]^{6-}$ chains are linked together by O(13) oxygen atoms creating an infinite ribbon $^1_\infty[U_2O_8]^{4-}$ (Fig. 4a). Each $U(1)O_7$ pentagonal bipyramid is sharing two opposite equatorial edges O(11)–O(10) with two $U(4)O_7$ pentagonal bipyramids to form a $[U_3O_{17}]^{16-}$ trimer, which is connected to two octahedra $U(2)O_6$ by sharing a two O(6)–O(11) edge to create a pentameric unit $[U_5O_{24}]^{18-}$ (Fig. 4b). These uranyl pentameric groups are connected together by sharing edges to form an infinite three polyhedra wide ribbon $^1_\infty[U_5O_{21}]^{12-}$ (Fig. 4b). Finally a puckered layers $^2_\infty[U_9O_{31}]^{8-}$ parallel to the (010) plane is obtained by sharing equatorial edges O(6)–O(15) and O(8)–O(15) between $U(4)O_7$ pentagonal bipyramids of $^1_\infty[U_5O_{21}]^{12-}$ ribbons on one side and distorted octahedra $U(3)O_6$ and $U(5)O_6$ of $^1_\infty[U_2O_8]^{4-}$ ribbons on other side (Fig. 4c). The $^1_\infty[U_2O_8]^{4-}$ ribbon is part of the $M_2U_2O_7$ (M = K, Rb) diuranate sheets whereas the $^1_\infty[U_5O_{21}]^{12-}$ ribbon is part of sheet found, for example, in $USbO_5$ [40] with commonly adopted uranophane sheet anion topology. Thus, the sheet in $Rb_8U_9O_{31}$ can be described as an ordered intergrowth of parts of the two types of sheets. The $^1_\infty[U_5O_{21}]^{12-}$ ribbons are also observed in $Sr_3U_{11}O_{36}$ [41], where layers result from the combination of

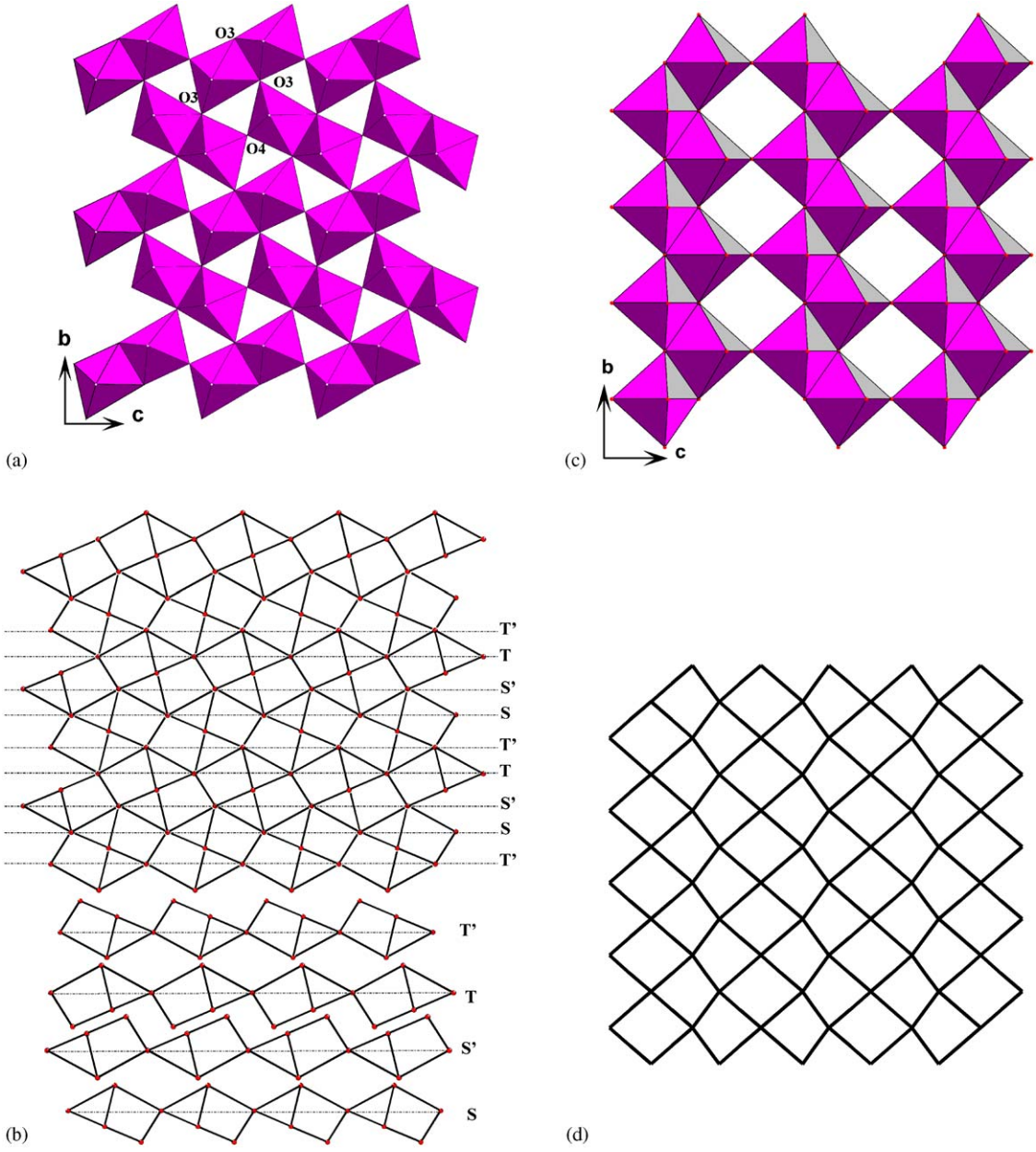

Fig. 1. Comparison of the $^{2}_{\infty}[U_2O_7]^{2-}$ layers built from edges and corners—sharing UO_6 octahedra, (a) in $M_2U_2O_7$, (M = K, Rb) and (c) in $M_2U_2O_7$. The sheet anion topology that contains squares and triangles can be described from arrowed chains **S**, **S′**, **T** and **T′** in $(K–Rb)_2U_2O_7$ (b), and from Autunite-type sheet in $Cs_2U_2O_7$ (d).

$^{1}_{\infty}[U_5O_{21}]^{12-}$ ribbons with $^{1}_{\infty}[Sr_3U_2O_{11}]^{4-}$ ribbons where the pentagonal U atoms are replaced Sr connected through chains similar to those observed in α-U_3O_8 [42]. In terms of chains the stacking sequence of nine chains is **TT′RDRURDR** where the chains denoted by **R**, **U**, **D** were defined by Miller et al. [43]. Note that $Cs_4U_5O_{17}$ [5–7] can be described by the five-chains sequence $(\mathbf{TT'RDR})_2$.

The $^{2}_{\infty}[U_9O_{31}]^{8-}$ corrugated layers are stacked along the (010) direction and the rubidium ions are located between the layers and hold them together (Fig. 5a). In this structure, two consecutive layers $^{2}_{\infty}[U_9O_{31}]^{8-}$ are deduced one after the other by an inversion center to give a unit cell with two infinite layers. There are four distinct rubidium atoms coordinated by six oxygen atoms forming distorted octahedra for Rb(1), Rb(2) and Rb(3) and a distorted trigonal prism for Rb(4) involving oxygen atoms that belong to the $U(3)O_2^{2+}$ and $U(5)O_2^{2+}$ uranyl groups of the $^{1}_{\infty}[U_2O_8]^{4-}$ ribbon. The RbO_6 polyhedra are edge shared to form a dense layer which is built from CdI_2-type octahedra ribbons, three octahedra width, connected through RbO_6 trigonal prisms. Within this layer some trigonal sites are empty and the formula of the layer is $Rb_8\square O_9$ (Fig. 5b).

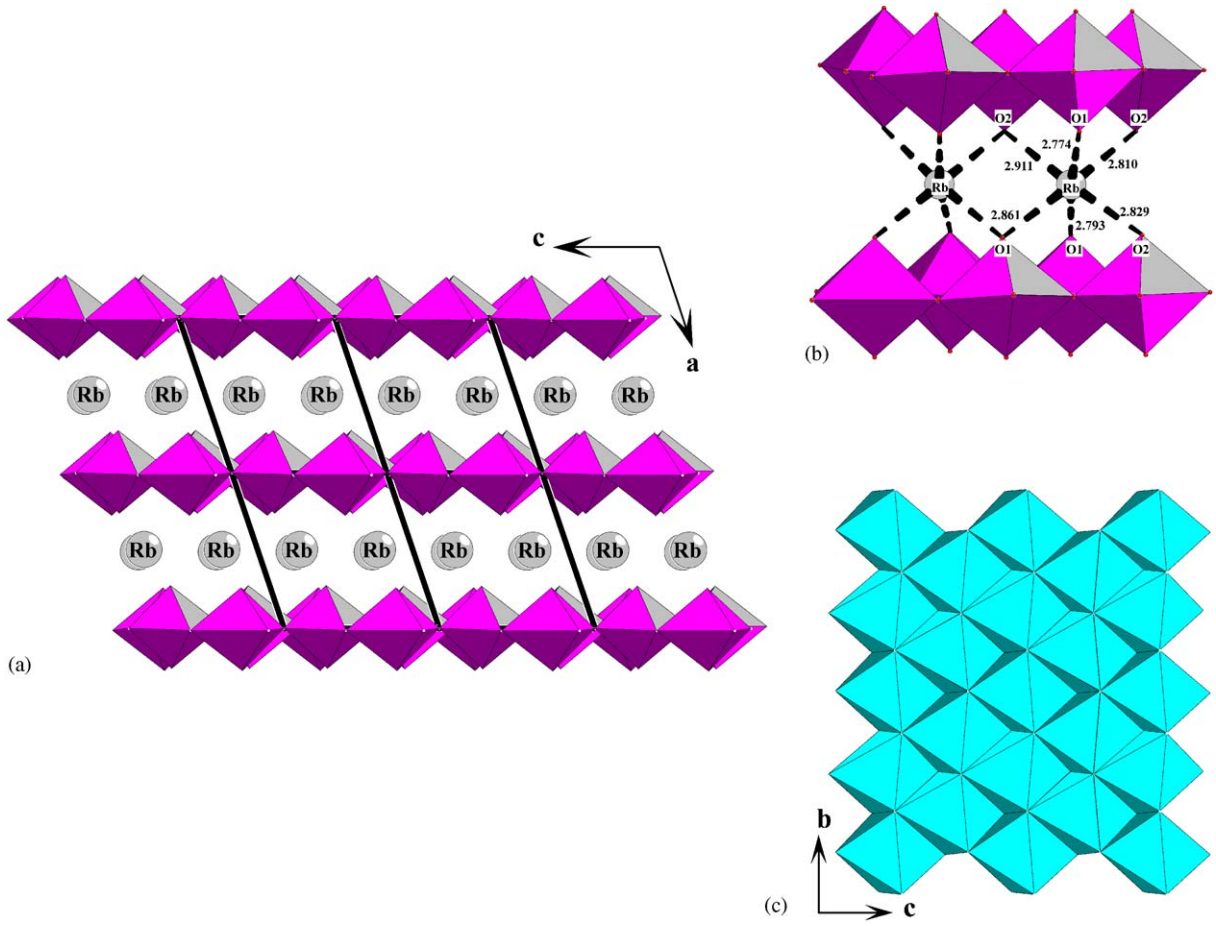

Fig. 2. (a) Stacking of $^{2}_{\infty}[U_2O_7]^{2-}$ layers in $Rb_2U_2O_7$ and occupation of the interlayer space by Rb^+ ions, (b) Octahedral coordination of the Rb^+ ions by uranyl oxygen atoms and (c) the dense RbO_2 layer of edge-shared TbO_6 octahedra.

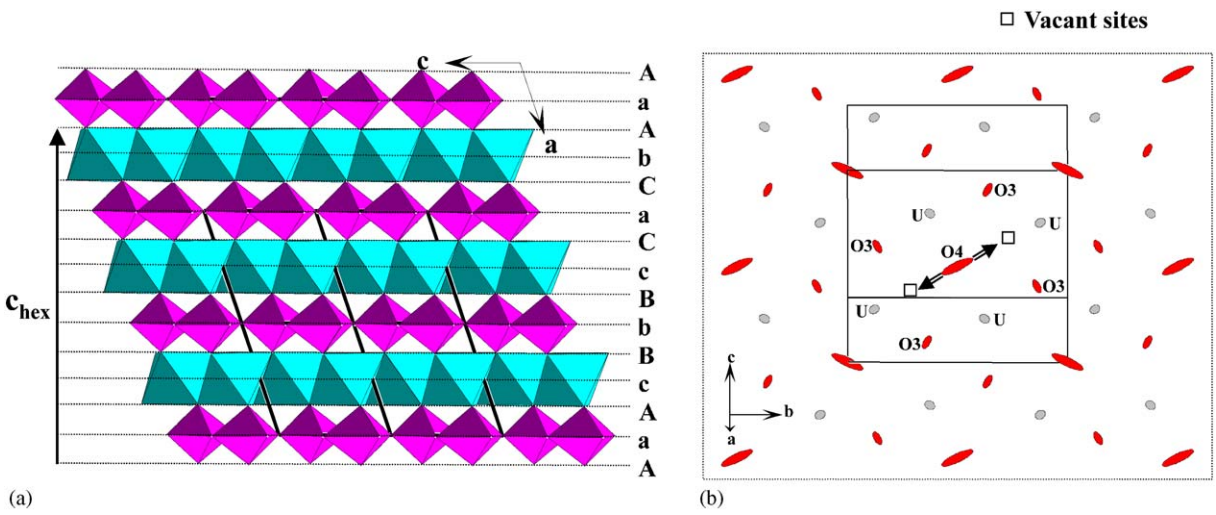

Fig. 3. (a) The crystal structure of $Rb_2U_2O_7$ described as a stacking of **AABBCC** of hexagonal-type oxygen layers, with octahedral *abc* sites occupied to form an octahedral shared RbO_2 layer. (b) The interspace between two identical hexagonal type oxygen layers are occupied by UO1.5 layers formed by U, O(3) and O(4) atoms.

Table 10
Interatomic distances (Å), valence bond and uranium–oxygen angles (°) in $Rb_8U_9O_{31}$

U Environment					
		s_{ij}			
U1–O2[i]	1.816(14)	1.555	*Uranium–oxygen angles*		
U1–O2	1.816(14)	1.555	O2–U1–O2[i]	179.02(64)	
U1–O11	2.237(13)	0.689	O2–U1–O11	90.64(52)	
U1–O11[i]	2.237(13)	0.689	O2–U1–O11[i]	88.68(52)	
U1–O4[ii]	2.361(14)	0.553	O2–U1–O4[ii]	90.49(38)	
U1–O10[iii]	2.566(14)	0.37	O2–U1–O10[iii]	90.22(53)	
U1–O10[ii]	2.566(14)	0.37	O2–U1–O10[ii]	90.18(53)	
$\sum s_{ij}$		**5.781**			
		s_{ij}			
U2–O9	1.845(15)	1.484	*Uranium–oxygen angles*		
U2–O3	1.848(15)	1.484	O9–U2–O3	177.53(64)	
U2–O4	2.181(6)	0.777	O9–U2–O4	92.30(51)	
U2–O6	2.185(13)	0.781	O9–U2–O6	91.98(60)	
U2–O10	2.226(13)	0.707	O9–U2–O10	89.48(57)	
U2–O11	2.240(13)	0.704	O9–U2–O11	91.87(55)	
$\sum s_{ij}$		**5.937**			
		s_{ij}			
U3–O12	1.811(14)	1.576	*Uranium–oxygen angles*		
U3–O7	1.815(14)	1.573	O12–U3–O7	178.18(64)	
U3–O6	2.180(13)	0.775	O12–U3–O6	89.89(62)	
U3–O15	2.215(13)	0.732	O12–U3–O15	90.21(60)	
U3–O8	2.224(13)	0.711	O12–U3–O8	90.39(56)	
U3–O13	2.289(13)	0.63	O12–U3–O13	89.68(61)	
$\sum s_{ij}$		**5.997**			
		s_{ij}			
U4–O5	1.781(13)	1.669	*Uranium–oxygen angles*		
U4–O1	1.817(13)	1.573	O1–U4–O5	175.83(58)	
U4–O10[ii]	2.189(13)	0.774	O1–U4–O6	88.83(49)	
U4–O6	2.345(12)	0.563	O1–U4–O8[ii]	86.15(51)	
U4–O8[ii]	2.368(13)	0.548	O1–U4–O15	89.49(56)	
U4–O15	2.444(14)	0.464	O1–U4–O11	92.10(51)	
U4–O11	2.521(13)	0.404	O1–U4–O10[ii]	91.19(55)	
$\sum s_{ij}$		**5.995**			
		s_{ij}			
U5–O16	1.813(14)	1.576	*Uranium–oxygen angles*		
U5–O14[vii]	1.840(13)	1.525	O16–U5–O14[vii]	174.48(61)	
U5–O15	2.150(13)	0.831	O16–U5–O15	93.47(58)	
U5–O13[ii]	2.274(12)	0.644	O16–U5–O13[ii]	90.72(52)	
U5–O13[viii]	2.287(13)	0.643	O16–U5–O13[viii]	89.22(53)	
U5–O8[ii]	2.298(13)	0.615	O16–U5–O8[ii]	90.34(53)	
$\sum s_{ij}$		**5.834**			
Rb environment					
		s_{ij}			s_{ij}
Rb1–O1[x]	2.746(14)	0.272	Rb2–O5	2.757(13)	0.260
Rb1–O2[iv]	2.747(13)	0.276	Rb2–O3[x]	2.766(15)	0.254
Rb1–O3[x]	2.765(13)	0.255	Rb2–O9	2.884(14)	0.186
Rb1–O3[i]	2.778(16)	0.247	Rb2–O7[x]	2.903(16)	0.177
Rb1–O9	2.878(15)	0.189	Rb2–O1[xii]	2.955(12)	0.151
Rb1–O2[xi]	2.871(14)	0.193	Rb2–O2	3.055(14)	0.115
$\sum s_{ij}$		**1.432**			**1.143**
		s_{ij}			s_{ij}
Rb3–O12	2.752(15)	0.265	Rb4–O12	2.818(15)	0.224
Rb3–O1[x]	2.892(13)	0.181	Rb4–O16	2.831(14)	0.217
Rb3–O14[v]	2.895(16)	0.179	Rb4–O14[ix]	2.839(13)	0.205
Rb3–O5[iv]	2.908(13)	0.177	Rb4–O7[x]	2.965(16)	0.144
Rb3–O7[x]	2.937(14)	0.164	Rb4–O16[vi]	3.006(14)	0.134
Rb3–O9	2.983(16)	0.141	Rb4–O14[xiii]	3.100(16)	0.102
$\sum s_{ij}$		**1.107**			**1.026**

Symmetry codes: (i) $x, 0.5-y, -z$; (ii) $-1+x, y, z$; (iii) $-1+x, 0.5-y, -z$; (iv) $1+x, y, z$; (v) $1-x, -0.5+y, z$; (vi) $0.5+x, y, 0.5-z$; (vii) $x, -1+y, z$; (viii) $-0.5+x, y, 0.5-z$; (ix) $-x, -0.5+y, z$; (x) $1-x, 0.5+y, z$; (xi) $1-x, 1-y, -z$; (xii) $-x, 0.5+y, z$; (xiii) $0.5-x, -0.5+y, 0.5-z$; (xiv) $x, 1+y, z$; (xv) $0.5-x, 0.5+y, 0.5-z$.

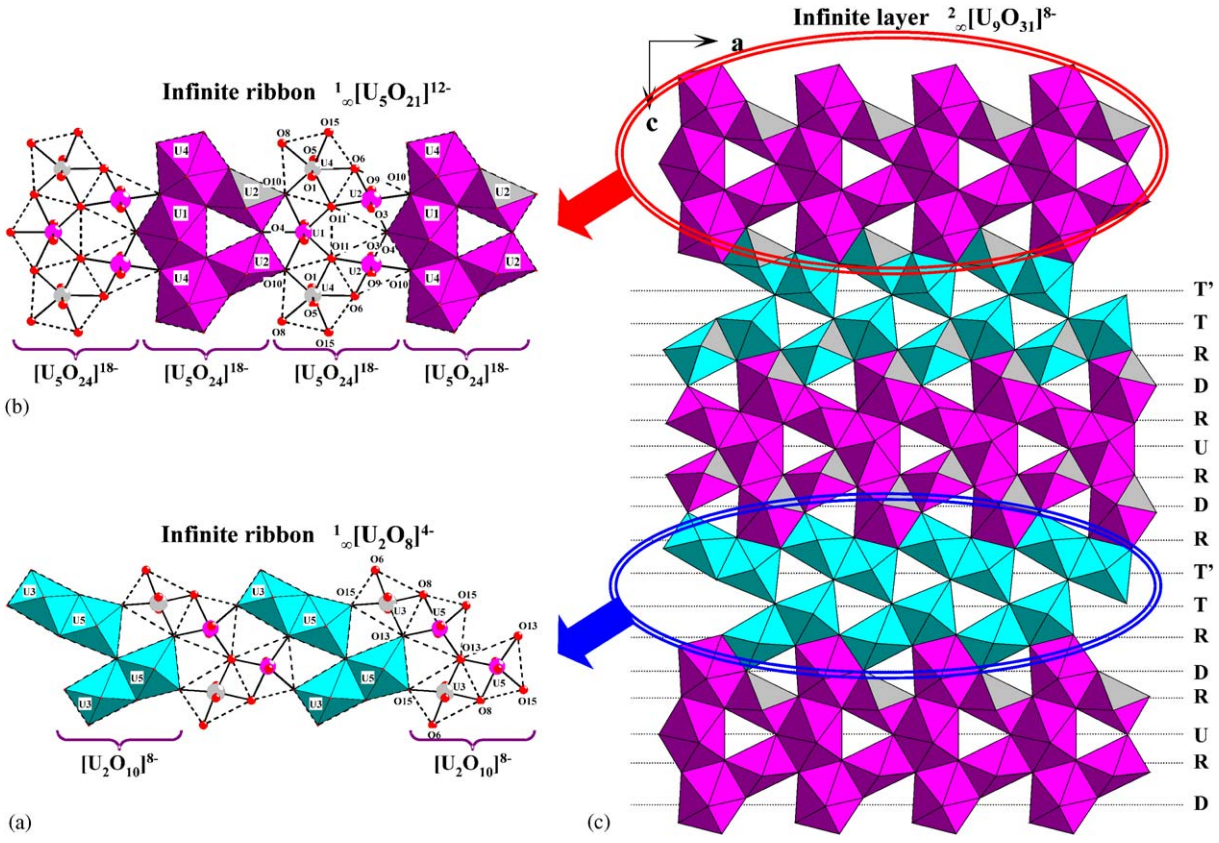

Fig. 4. The $^{2}_{\infty}[U_9O_{31}]^{8-}$ infinite layer in $Rb_8U_9O_{31}$ (c) which can be described as the intergrowth of $^{1}_{\infty}[U_5O_{21}]^{12-}$ ribbons of uranophane sheet anion topology (b) and $^{1}_{\infty}[U_2O_8]^{4-}$ ribbons similar to that found in $Rb_2U_2O_7$ (a).

3.4. Electrical properties

The layered structure of $Rb_2U_2O_7$ and $Rb_8U_9O_{31}$ compounds allows us to consider some mobility of the alkali metal cations localized in interlayer spaces. Thus, Fig. 6 indicates the temperature dependence of the conductivity for the two compounds. The electrical measurements show that the conductivity obeys to the Arrhenius law in the studied temperature domain, with a linear evolution of $\log\sigma$ according to $1/T$. Both studied compounds exhibit low and comparable conductivity with activation energies about 0.81 and 0.85 eV for $Rb_2U_2O_7$ and $Rb_8U_9O_{31}$, respectively. The low conductivity and high activation energy observed in both compounds may be explained by the fact that there is a direct relation between structural aspect and electric conductivity. Indeed, in these two structures the Rb^+ ions are not very mobile because of their size, and particularly of the rigidity of their octahedral environment where the rubidium atoms in interlayer spaces are strongly linked to the uranyl layers with almost Rb–O distances lower than 2.90 Å and finally the lack of partially occupied rubidium sites.

No transition or melting point has been observed on the DTA experiments. The X-ray powder diffraction analyses of residues after each DTA measurement showing that both phases are stable until 1300 °C. These observations confirm the high thermal stability of uranates.

3.5. Spectroscopic properties

For both compounds the infrared spectrum (400–1000 cm^{-1}) (Fig. 7), is characterized by two vibration domains, corresponding to [O═U═O] uranyl ions and U–O equatorial vibrations. Thus, to interpret the IR spectrum two following building units have been considered: UO_2^{2+} groups and equatorial (secondary) U–O bonds. For $Rb_2U_2O_7$, the spectrum shows two strong bands at about 807 and 745 cm^{-1}, which can be attributed to asymmetrical and symmetrical UO_2^{2+} uranyl stretching vibrations ν_3 and ν_1, respectively, for uranyl ion in octahedral coordination, in good agreement with Volkovich et al. infrared investigation [44]. However, in $Rb_8U_9O_{31}$, two asymmetrical and symmetrical vibrations couples (805, 740) and (835, 760) cm^{-1} have been observed, corresponding to (ν_3, ν_1) vibration bands of uranyl ions in octahedral and pentagonal bipyramid environments, respectively. For both spectra, the (ν_3, ν_1) vibration bands values are in

good agreement with the mathematical model suggested by Bagnall and Wakerley [45] to determine the value of v_1 from that of v_3, $v_1 = 0.912v_3 - 1.04\,(cm^{-1})$.

The application of Veal et al.'s empirical equation [46], relating bond length (d) to the asymmetric stretching vibration v_3 for uranyl groups, $d_{U-O} = 81.2v_3^{-2/3} + 0.895$, leads to the predicted uranyl bond length, in good agreement with the average value obtained from X-ray structure results (Table 11). The lower bands observed in the range 440–650 cm^{-1} may be assigned to the U–O_{eq} vibrations between uranium and equatorial oxygen atoms, these bands were also observed in other mineral and inorganic compounds [47]. A summary of the assignment of absorption bands is also given for both compounds in Table 11.

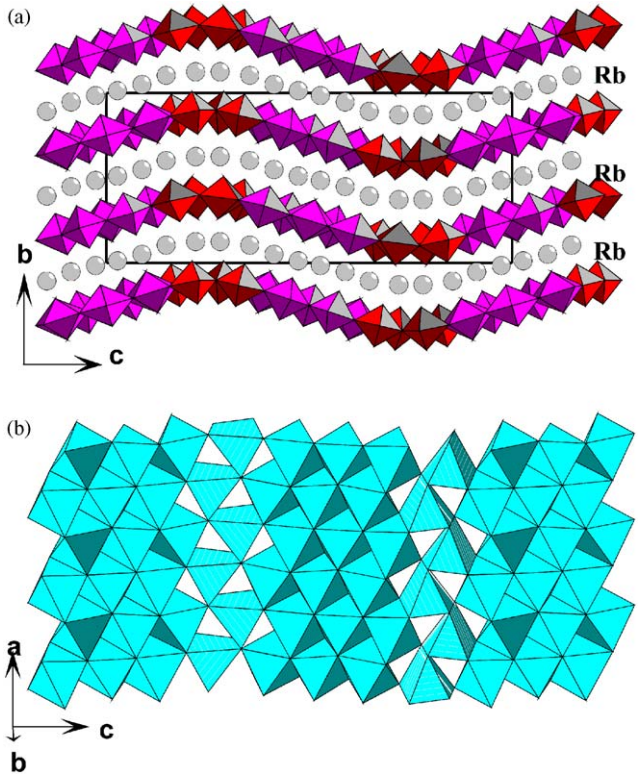

Fig. 5. Stacking of $^{2}_{\infty}[U_9O_{31}]^{8-}$ layers $Rb_8U_9O_{31}$ with Rb^+ ions in interlayer spaces (a), forming with uranyl oxygen a puckered layer $Rb_8\square O_9$ (b).

4. Conclusion

The structures of the diuranate $Rb_2U_2O_7$ and the new uranate in $Rb_8U_9O_{31}$ contains bi-dimensional layers of uranyl polyhedra connected by edges and corners. In $Rb_2U_2O_7$ the layer is built from UO_6 distorted octahedra and is planar, the rubidium polyhedra forming an hexagonal sheet of edge-shared octahedra of CdI_2-type. The addition in the formula of supplementary UO_3 units from $Rb_2U_2O_7$ ($Rb_8U_8O_{28}$) to $Rb_8U_9O_{31}$ ($Rb_8U_8O_{28} + UO_3$) and the previously reported $Cs_4U_5O_{17}$ ($Cs_8U_8O_{28} + 2UO_3$) introduce UO_7 pentagonal bipyramids in the U–O sheet and induce the replacement of some octahedra by trigonal prism in the Rb–O sheet which can be considered as lacunar Rb_8O_{16}, $Rb_8\square O_{18}$, and $Cs_8\square_2O_{20}$, in $Rb_2U_2O_7$, $Rb_8U_9O_{31}$, and $Cs_4U_5O_{17}$, respectively. This structural filiation encourages us to take again the investigation of the M–U–O diagrams with modern characterization methods such as electronic microscopy to evidence new phases and to rule on certain still discussed results.

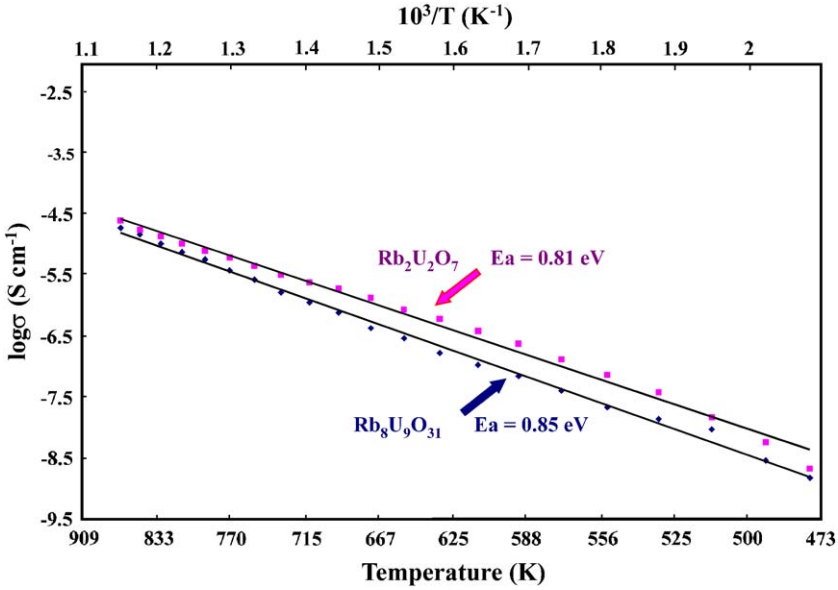

Fig. 6. Comparison between $Rb_2U_2O_7$ and $Rb_8U_9O_{31}$ cationic conductivity vs. temperature.

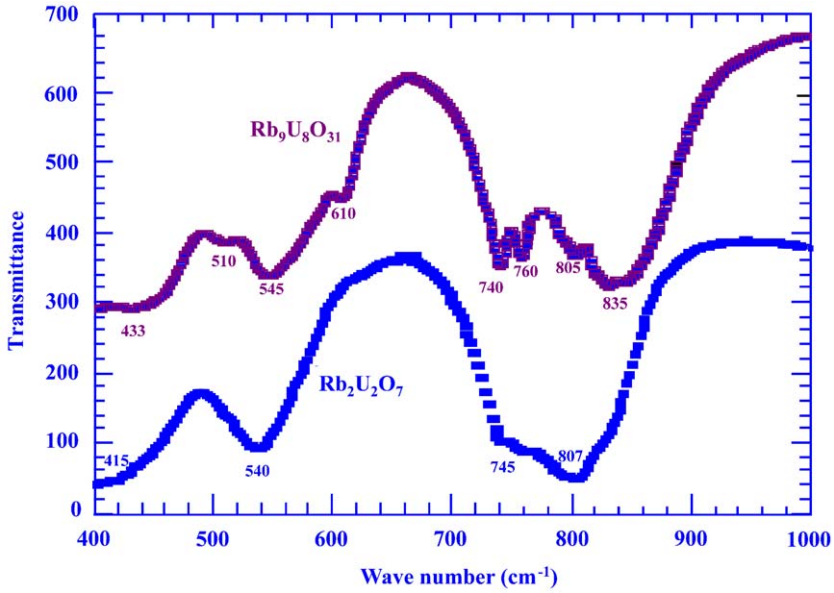

Fig. 7. Infrared spectra of $Rb_2U_2O_7$ and $Rb_8U_9O_{31}$.

Table 11
Vibration Bands in infrared spectrum, and calculated uranyl distances d_{U-O} (Å) for $Rb_2U_2O_7$ and $Rb_8U_9O_{31}$

	$Rb_8U_9O_{31}$	d_{U-O}	$Rb_2U_2O_7$	d_{U-O}
ν_3 (cm^{-1})	835(S)	1.81		
Asymmetric stretch.	805(m)	1.83	807(S)	1.83
ν_1 (cm^{-1})	760(m)		745(m)	
Symmetric stretch.	740(S)			
U–O equatorial and *M*–O	610(m)			
	545(S)	540(S)		
	510(w)			
	433(m)	415(w)		

References

[1] T.R. Griffiths, V.A. Volkovich, J. Nucl. Mater. 274 (3) (1999) 229.
[2] A.B. Van Egmond, Sticht. React. Cent. Ned., Petten, Neth. Avail INIS Report 1976, INIS-mf-3173, 124pp. (From: INIS Atomindex 7(20) (1976) Abstr. No. 268064).
[3] E.H.P. Cordfunke, A.B. Van Egmond, G. Van Woorst, J. Inorg. Nucl. Chem. 37 (6) (1975) 1433.
[4] A.B. Van Egmond, J. Inorg. Nucl. Chem. 38 (11) (1976) 2105.
[5] A.B. Van Egmond, J. Inorg. Nucl. Chem. 38 (9) (1976) 1649.
[6] S. Van den Berghe, J.P. Laval, B. Gaudeau, H. Terryn, M. Verwerft, J. Nucl. Mater. 277 (2000) 28.
[7] S. Van den Berghe, M. Verwerft, J.P. Laval, B. Gaudeau, P.G. Allen, A. Van Wyngarden, J. Solid State Chem. 166 (2002) 320.
[8] S. Van den Berghe, J.P. Laval, M. Verwerft, B. Gaudeau, E. Suard, Solid State Sci. 4 (2002) 1257.
[9] A.B. van Egmond, E.H.P. Cordfunke, J. Inorg. Nucl. Chem. 38 (12) (1976) 2245.
[10] L.M. Kovba, Zh. Strukt. Khim. 13 (2) (1972) 256–259.
[11] L.M. Kovba, V.I. Trunova, Radiokhimiya 13 (5) (1971) 773.
[12] L.M. Kovba, E.A. Ippolitova, Yu.P. Smanov, V.I. Spitsyn, Dokl. Akad. Nauk SSSR 120 (1958) 1042.
[13] L.M. Kovba, I.A. Murav'eva, A.S. Orlova, Radiokhimiya 16 (5) (1974) 648.
[14] E.H.P. Cordfunke, D.J.W. Ijdo, J. Solid State Chem. 115 (1995) 299.
[15] F.C. Mijlhoff, D.J.W. Ijdo, E.H.P. Cordfunke, J. Solid State Chem. 102 (2) (1993) 299.
[16] C.J. Toussaint, A. Avogadro, J. Inorg. Nucl. Chem. 36 (4) (1974) 781.
[17] L.M. Kovba, Zh. Strukt. Khim. 13 (2) (1972) 256.
[18] N.C. Jayadevan, K.D. Singh Mudher, D.M. Chackraburthy, BARC-report-726, India, Bombay, 1974.
[19] J. Jove, A. Cousson, J. Less-Common Met. 139 (1988) 345.
[20] M.C. Saine, J. Less-Common Met. 154 (1989) 361.
[21] K.M. Efremova, E.A. Ippolitova, Yu.P. Simanov, in: Issledovaniya v Oblasti Khimii Urana, Sbornik Stateii, Mosk. Gos. Univ., Moscow, 1961, pp. 50–55.
[22] K.L. Chawla, N.L. Misra, N.C. Jayadevan, J. Inorg. Nucl. Chem. 154 (2–3) (1988) 181.
[23] G. Prins, E.H.P. Cordfunke, J. Less-Common Met. 91 (2) (1983) 177.
[24] J. Hauck, J. Inorg. Nucl. Chem. 36 (10) (1974) 2291.
[25] J. Hauck, J. Z. Naturforsch. 28 (3–4) (1973) 215.
[26] E. Gebert, H.R. Hoekstra, A.H. Reis, S.W. Peterson, J. Inorg. Nucl. Chem. 40 (1) (1978) 65.
[27] V.I. Spitsyn, E.A. Ippolitova, K.M. Efremova, Yu.P. Simanov, in: Issledovaniya v Oblasti Khimii Urana, Sbornik Stateii, Mosk. Gos. Univ., Moscow, 1961, pp. 121–125.
[28] K.M. Efremova, E.A. Ippolitova, Yu.P. Simanov, V.I. Spitsyn, Dokl. Akad. Nauk SSSR 124 (1959) 1057.
[29] J.G. Allpress, J.S. Anderson, A.N. Hambly, J. Inorg. Nucl. Chem. 30 (5) (1968) 1195.
[30] S. Obbade, S. Yagoubi, C. Dion, M. Saadi, F. Abraham, J. Solid State Chem. 174 (2003) 19.
[31] SAINT, Program for reduction of data collected on Bruker AXS CCD area detector system, Bruker Analytical X-ray Systems, Madison, WI, 1998.

[32] G.M. Sheldrick, SHELXTL NT, Program Suite for solution and Refinement of Crystal Structure, version 5.1, Bruker Analytical X-ray Systems, Madison, WI, 1998.
[33] SABABS, Program for absorption correction using SMART CCD based on the method of Blessing: Blessing, R.H., Acta Crystallogr. A 51 (1995) 33.
[34] G.M. Sheldrick, SHELXS-86, Program for Crystal Structure Determination, University of Göttingen, Germany, 1986.
[35] M.E. Brese, M. O'Keeffe, Acta Crystallogr. B 47 (1991) 192.
[36] P.C. Burns, R.C. Ewing, F.C. Hawthorne, Can. Mineral. 35 (1997) 1551.
[37] G. Smith, R.J. Snyder, J. Appl. Crystallogr. 12 (1979) 60.
[38] P.C. Burns, M. Miller, R.C. Ewing, Can. Mineral. 34 (1996) 845.
[39] R.J. Traill, Can. Mineral. 7 (1962) 524.
[40] P.G. Dickens, G.P. Stuttard, J. Mater. Chem. 2 (1992) 691.
[41] E.H.P. Cordfunke, P. Van Vlaanderen, M. Onink, D.J.W. IJdo, J. Solid State Chem. 94 (1991) 12.
[42] B.O. Loopstra, Acta Crystallogr. B 26 (1970) 656.
[43] M.L. Miller, R.J. Finch, P.C. Burns, R.C. Ewing, J. Mater. Res. 11 (1996) 3048.
[44] V.A. Volkovich, T.R. Griffiths, R.C. Thied, Vibr. Spectrosc. 25 (2) (2001) 223.
[45] K.W. Bagnall, M.W. Wakerley, J. Inorg. Nucl. Chem. 37 (1) (1975) 329.
[46] B.W. Veal, D.J. Lam, W.T. Carnall, H.R. Hestra, Phys. Rev. B (1975) 5651.
[47] J. Cejka, Rev. Miner. 38 (1999) 221.